 SDHM, vol.5, no.3, pp.191-199, 2009

# Generalized Stress Intensity Factors for Wedge-Shaped Defect in Human Tooth after Restored with Composite Resins

**Kyousuke Yamaguchi[1], Nao-Aki Noda[2], Ker-Kong Chen[3], Kiyoshi Tajima[3] Seiji Harada[1] and Xin Lan[1]**

**Abstract:** Wedge-shaped defects are frequently observed on the cervical region of the human tooth. Previously, most studies explained that improper toothbrushing causes such defects. However, recent clinical observation suggested that the repeated stress due to occlusal force may induce the formation of these wedge-shaped defects. In this study, a two-dimensional human tooth model after a wedge-shaped defect is restored with the composite resin is analyzed by using the finite element method. To obtain the intensity of the singular stress accurately, a method of analysis is discussed for calculating generalized stress intensity factors, which control the singular stress around the corner of inclusion. In this study, elastic module ratios of the composite resin are varied systematically. Then, the relationships between the stress intensity and occlusion are discussed.

**Keywords:** Elasticity, Biomechanics, Fracture Mechanics, Finite Element Method, Wedge-Shaped Defect, Human Tooth

## 1 Introduction

Wedge-shaped defects as shown in Fig.1 are frequently observed on the cervical region of the human tooth. Such types of defects are more frequently observed for aging people. Therefore to establish a remedy will become more important in aging societies, this is appearing in Japan and many other countries in the near future.

Early research by Miller showed that wedge-shaped defect is affected by hard toothbrushes, and that opinion has been accepted for a long time [Miller (1907)]. Later,

[1] Department of Mechanical Engineering, Kyushu Institute of Technology, 1-1 Sensui-cho, Tobata-ku,Kitakyushu, 804-8550 Japan

[2] Kyushu Institute of Technology, Department of Mechanical Engineering E-mail address: noda@mech.kyutech.ac.jp

[3] Kyushu Dental College 2-6-1 Manazuru,Kokurakita-ku,Kitakyushu,803-8580 Japan

Bream et al found wedge-shaped defect at the region of human mouth [Bream et al (1992)] which are hard to brush. Similarly, Graehn confirmed wedge-shaped defect in the animal tooth [Graehn et al]. Odera and Tanaka reported that the wedge-shaped defect exist in the ancients that had not used toothbrush [Tanaka et al (1993)]. The above studies suggest that improper toothbrushes cannot be the only reason for wedge-shaped defects.

Lee and Eakle suggested that when occlusion is not ideal the tensile stress due to lateral forces may disrupt the chemical bonds of the crystalline structure of enamel and dentin [Lee and Eakle (1984)]. Recently, Chen et al used the maxillary second premolar and measured the strain to find out the potential relationship between occlusion and wedge-shaped defect [Chen et al (2000)].

Generally, the singular stress around the corner of wedge-shaped inclusions is expressed as shown in Eq.1 [Chen and Nishitani (1991)]. In this study, the finite element method is applied and the intensity of the singular stress at the corner of wedge-shaped inclusion will be calculated accurately. Then, the effect of the occlusal force will be discussed.

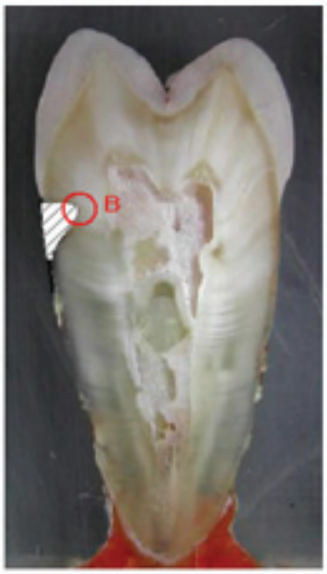


Figure 1: Wedge-shaped defect filled with composite resin

## 2 Analysis for generalized stress intensity factors (GSIF) by the application of the finite element method

### 2.1 Singular stress field for corner B

It is confirmed by clinical observation that wedge-shaped defect restored by the composite resin can be destructed from corner B shown in Fig.2. In order to investigate this problem from the viewpoint of mechanics, it is necessary to study the singular stress field for the corner B. First, the problem of Fig.2 (b) is studied to confirm the usefulness of the present solution. Then, the relationships between the stress intensity and occlusion are discussed. The singular stress field for corner B in Fig.2 can be expressed in Eq.1.

$$\sigma_{ij} = \frac{K_{\mathrm{I},\lambda_1}}{r^{1-\lambda_1}} f_{ij}^{\mathrm{I}}(\theta) + \frac{K_{\mathrm{II},\lambda_2}}{r^{1-\lambda_2}} f_{ij}^{\mathrm{II}}(\theta) \quad , \qquad ij = r,\theta,r\theta \tag{1}$$

$$K_{\mathrm{I},\lambda_1} = F_{\mathrm{I},\lambda_1}\sigma\sqrt{\pi}l^{1-\lambda_1}, \quad K_{\mathrm{II},\lambda_2} = F_{\mathrm{II},\lambda_2}\sigma\sqrt{\pi}l^{1-\lambda_2} \tag{2}$$

Where, $K_{\mathrm{I},\lambda_1}$, $K_{\mathrm{II},\lambda_2}$ are stress intensity factors of model I and model II respectively, $F_{\mathrm{I},\lambda_1}$, $F_{\mathrm{II},\lambda_2}$ are non-dimensional stress intensity factors. The following equations (3) (4) (5) (6) are used to calculate the values of $f_{ij}^{\mathrm{I}}(\theta)$ and $f_{ij}^{\mathrm{II}}(\theta)$.

$$\begin{aligned} f_{\theta}^{\mathrm{I}}(\theta) = & \frac{\lambda_1}{\sqrt{2\pi(\alpha-\beta)}} \left[ \left[ \lambda_1(\alpha-\beta)\sin\{\gamma-\lambda_1(\gamma-\pi)\} + (1-\beta)\sin(\lambda_1\pi) \right] \right. \\ & \times \cos\{(\lambda_1+1)\theta\} \\ & \left. + \left[ (\lambda_1+1)\times(\alpha-\beta)\sin\{\lambda_1(\gamma-\pi)\} \right] \times \cos\{(\lambda_1-1)\theta\} \right] \end{aligned} \tag{3}$$

$$\begin{aligned} f_{\theta}^{\mathrm{II}}(\theta) = & \frac{\lambda_2}{\sqrt{2\pi(\alpha-\beta)}} \left[ \left[ \lambda_2(\alpha-\beta)\sin\{\gamma-\lambda_2(\gamma-\pi)\} + (1-\beta)\sin(\lambda_2\pi) \right] \right. \\ & \times \sin\{(\lambda_2+1)\theta\} \\ & \left. + \left[ (\lambda_2+1)\times(\alpha-\beta)\sin\{\lambda_2(\gamma-\pi)\} \right] \times \sin\{(\lambda_2-1)\theta\} \right] \end{aligned} \tag{4}$$

$$\begin{aligned} f_{r\theta}^{\mathrm{I}}(\theta) = & \frac{\lambda_1}{\sqrt{2\pi(\alpha-\beta)}} \left[ \left[ \lambda_1(\alpha-\beta)\sin\{\gamma-\lambda_1(\gamma-\pi)\} + (1-\beta)\sin(\lambda_1\pi) \right] \right. \\ & \times \sin\{(\lambda_1+1)\theta\} \\ & \left. + \left[ (\lambda_1+1)\times(\alpha-\beta)\sin\{\lambda_1(\gamma-\pi)\} \right] \times \sin\{(\lambda_1-1)\theta\} \right] \end{aligned} \tag{5}$$

$$\begin{aligned} f_{r\theta}^{\mathrm{II}}(\theta) = & \frac{\lambda_2}{\sqrt{2\pi(\alpha-\beta)}} \left[ \left[ \lambda_2(\alpha-\beta)\sin\{\gamma-\lambda_2(\gamma-\pi)\} + (1-\beta)\sin(\lambda_2\pi) \right] \right. \\ & \times \cos\{(\lambda_2+1)\theta\} \\ & \left. + \left[ (\lambda_2+1)\times(\alpha-\beta)\sin\{\lambda_2(\gamma-\pi)\} \right] \times \cos\{(\lambda_2-1)\theta\} \right] \end{aligned} \tag{6}$$

Furthermore, $F_{\theta B}|_{\theta=0}$, $F_{r\theta B}|_{\theta=\pm 150^\circ}$ are introduced to define the value of singular stresses $\sigma_{\theta B}$, $\tau_{r\theta B}$ in corner B. Namely,

$$\sigma_{ij} = \frac{K_{\mathrm{I},\lambda_1}}{r^{1-\lambda_1}} f_{ij}^{\mathrm{I}}(\theta) + \frac{K_{\mathrm{II},\lambda_2}}{r^{1-\lambda_2}} f_{ij}^{\mathrm{II}}(\theta) = \frac{F_{ij}^{\mathrm{I}}}{r^{1-\lambda_1}} + \frac{F_{ij}^{\mathrm{II}}}{r^{1-\lambda_2}}, \quad ij = r, \theta, r\theta \tag{7}$$

Assume $E_M$ is Young's modulus of dentin and $E_I$ is Young's modulus of composite resin. When $E_I/E_M$<1, destruction happens on the bisector of the wedge-shaped defect since the stress concentration. Stresses $\sigma_{\theta B}|_{\theta=0^\circ}$ and $\tau_{\theta B}|_{\theta=0^\circ}$ are investigated and expressed by Eq. (8),(9).

$$\sigma_{\theta B}|_{\theta=0^\circ} = \frac{F_{\theta B}|_{\theta=0^\circ}}{r^{1-\lambda_1}} = \frac{K_{\mathrm{I},\lambda_1} f_\theta^{\mathrm{I}}(\theta)|_{\theta=0^\circ}}{r^{1-\lambda_1}} \tag{8}$$

$$\tau_{r\theta B}|_{\theta=0^\circ} = \frac{F_{r\theta B}|_{\theta=0^\circ}}{r^{1-\lambda_2}} = \frac{K_{\mathrm{II},\lambda_2} f_\theta^{\mathrm{II}}(\theta)|_{\theta=0^\circ}}{r^{1-\lambda_2}} \tag{9}$$

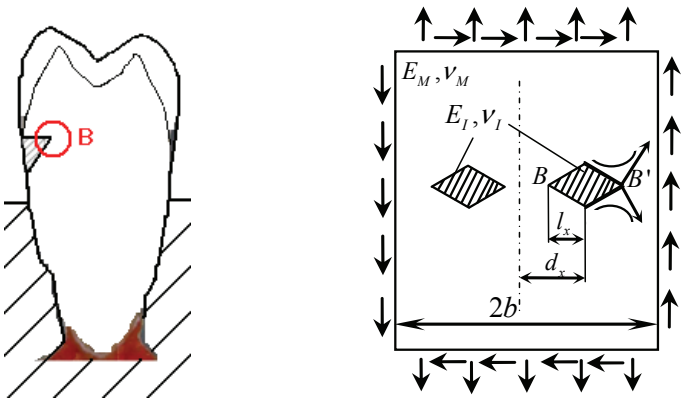


(a) Singular stress field for the corner B (b)Diamond-shaped inclusion for the corner B

Figure 2: Problem considered for the corner B

When $E_I/E_M$>1, destruction happens on the interface ($\theta = \pm 150^\circ$) of dentin and composite resin. Stresses $\sigma_{\theta B}|_{\theta=\pm 150^\circ}$ and $\tau_{\theta B}|_{\theta=\pm 150^\circ}$ are investigated and expressed by Eq. (10), (11), (12), (13).

For $\theta = 150^\circ$, then

$$\begin{aligned}\sigma_{\theta B}|_{\theta=150^\circ} &= \frac{F^{\mathrm{I}}_{\theta B}|_{\theta=150^\circ}}{r^{1-\lambda_1}} + \frac{F^{\mathrm{II}}_{\theta B}|_{\theta=150^\circ}}{r^{1-\lambda_2}} \\ &= \frac{K_{\mathrm{I},\lambda_1} f^{\mathrm{I}}_{\theta}(\theta)|_{\theta=150^\circ}}{r^{1-\lambda_1}} + \frac{K_{\mathrm{II},\lambda_2} f^{\mathrm{II}}_{\theta}(\theta)|_{\theta=150^\circ}}{r^{1-\lambda_2}}\end{aligned} \tag{10}$$

$$\begin{aligned}\tau_{r\theta B}|_{\theta=150^\circ} &= \frac{F^{\mathrm{I}}_{r\theta B}|_{\theta=150^\circ}}{r^{1-\lambda_1}} + \frac{F^{\mathrm{II}}_{r\theta B}|_{\theta=150^\circ}}{r^{1-\lambda_2}} \\ &= \frac{K_{\mathrm{I},\lambda_1} f^{\mathrm{I}}_{\theta}(\theta)|_{\theta=150^\circ}}{r^{1-\lambda_1}} + \frac{K_{\mathrm{II},\lambda_2} f^{\mathrm{II}}_{\theta}(\theta)|_{\theta=150^\circ}}{r^{1-\lambda_2}}\end{aligned} \tag{11}$$

For $\theta = -150^\circ$, then

$$\sigma_{\theta B}|_{\theta=-150^\circ} = \frac{F^{\mathrm{I}}_{\theta B}|_{\theta=-150^\circ}}{r^{1-\lambda_1}} - \frac{F^{\mathrm{II}}_{\theta B}|_{\theta=-150^\circ}}{r^{1-\lambda_2}} \tag{12}$$

$$\tau_{r\theta B}|_{\theta=-150^\circ} = \frac{F^{\mathrm{I}}_{r\theta B}|_{\theta=-150^\circ}}{r^{1-\lambda_1}} + \frac{F^{\mathrm{II}}_{r\theta B}|_{\theta=-150^\circ}}{r^{1-\lambda_2}} \tag{13}$$

### *2.2 Method of analysis*

Consider two diamond-shaped inclusions in a plate as shown in Fig.2. The generalized stress intensity factors in Eq 1 are evaluated for $l_x/d_x$ equal to 1/3, 1/2, and 2/3. The solutions are compared with the exact solutions obtained by the body force method [Noda et al (1996)]. In Ref Noda et al (1996), since only the results for $l_x/b \to 0$ are available, FEM results are extrapolated from the results of $l_x/b = 0.05,_0.1$.When $E_I/E_M$<1, the stress distributions along the bisector of the corner $\theta$=0$^\circ$ are considered (see Fig.2). When $E_I/E_M$>1, the interface stress distributions at $\theta = \pm 150^\circ$ are considered. In the analysis of FEM, the exact singular stress field cannot be given from finite numbers of elements. However, the error due to the finiteness of the division mainly depends on the mesh around the corner of the inclusion. Therefore if the generalized stress intensity factors are equal for different problems, the FEM stress distributions are also nearly equal if the same FEM mesh is applied around the corner. To calculate mode I stress intensity factors, $\sigma^*_{\theta,FEM}$is considered, and to calculate mode II stress intensity factors, $\tau^*_{r\theta,FEM}$is considered in a similar way.

- When $E_I/E_M$<1, stress distributions at $\theta = 0^\circ$ are considered.

$$\frac{K_{\mathrm{I},\lambda_1,real}}{\sigma_{\theta,FEM}|_{\theta=0}} = \frac{K^*_{\mathrm{I},\lambda_1,real}}{\sigma^*_{\theta,FEM}|_{\theta=0}}, \quad \frac{K_{\mathrm{I},\lambda_2,real}}{\tau_{r\theta,FEM}|_{\theta=0}} = \frac{K^*_{\mathrm{I},\lambda_2,real}}{\tau^*_{r\theta,FEM}|_{\theta=0}} \tag{14}$$

- When $E_I/E_M$>1, stress distributions at are considered.

$$\frac{K_{\mathrm{I},\lambda_1,real}}{\tau^{\mathrm{I}}_{r\theta,FEM}} = \frac{K^*_{\mathrm{I},\lambda_1,real}}{\tau^{\mathrm{I}*}_{\theta,FEM}}, \quad \frac{K_{\mathrm{I},\lambda_1,real}}{\sigma^{\mathrm{I}}_{\theta,FEM}} = \frac{K^*_{\mathrm{I},\lambda_1,real}}{\sigma^{\mathrm{I}*}_{\theta,FEM}} \tag{15}$$

$$\sigma^{\mathrm{I}}_{\theta} = (\,\sigma_\theta|_{\theta=150^\circ} + \sigma_\theta|_{\theta=-150^\circ})/2, \quad \tau^{\mathrm{I}}_{r\theta} = (\,\tau_{r\theta}|_{\theta=150^\circ} - \tau_{r\theta}|_{\theta=-150^\circ})/2 \tag{16}$$

$$\frac{K_{\mathrm{I},\lambda_2,real}}{\sigma^{\mathrm{I}}_{\theta,FEM}} = \frac{K^*_{\mathrm{I},\lambda_2,real}}{\sigma^{\mathrm{I}*}_{\theta,FEM}}, \quad \frac{K_{\mathrm{I},\lambda_2,real}}{\tau^{\mathrm{I}}_{r\theta,FEM}} = \frac{K^*_{\mathrm{I},\lambda_2,real}}{\tau^{\mathrm{I}*}_{r\theta,FEM}} \tag{17}$$

$$\sigma^{\mathrm{I}}_{\theta} = (\,\sigma_\theta|_{\theta=150^\circ} - \sigma_\theta|_{\theta=-150^\circ})/2, \quad \tau^{\mathrm{I}}_{r\theta} = (\,\tau_{r\theta}|_{\theta=150^\circ} + \tau_{r\theta}|_{\theta=-150^\circ})/2 \tag{18}$$

In these equations, the asterisks * mean the values of the reference problem for $l_x/b \to 0$ of which the exact solutions are available. Here, $K^*_{\mathrm{I},\lambda_1,real}$, $K^*_{\mathrm{I},\lambda_2,real}$ mean exact generalized stress intensity factors, and $\sigma^*_{\theta,FEM}\Big|_{\theta=0^\circ}$, $\tau^*_{r\theta,FEM}\Big|_{\theta=0^\circ}$ are the stresses along the bisector of the notch when the finite element method is applied to the same problems. If the following Eq. 19 is applied as the definition of non-dimensional stress intensity factor, Eq. 20 is given from Eq. 14.

$$F_{\mathrm{I},\lambda_1,real} = \frac{K_{\mathrm{I},\lambda_1}}{\sigma\sqrt{\pi}l^{1-\lambda_1}}, \quad F^*_{\mathrm{I},\lambda_1,BFM} = \frac{K^*_{\mathrm{I},\lambda_1}}{\sigma^*\sqrt{\pi}l^{*1-\lambda_1}} \tag{19}$$

$$\frac{F_{\mathrm{I},\lambda_1,real}\sigma\sqrt{\pi}l^{1-\lambda_1}}{\sigma_{\theta,FEM}} = \frac{F^*_{\mathrm{I},\lambda_1,BFM}\sigma^*\sqrt{\pi}l^{*1-\lambda_1}}{\sigma^*_{\theta,FEM}} \tag{20}$$

## 3 Results and Discussion

### *3.1 Results for two diamond-shaped inclusions*

General stress intensity factors for two diamond-shaped inclusions in a plate are calculated under different $l_x/d_x$ ratios ($l_x/d_x$=0.05, 0.1) using the Finite Element Method mentioned above, then the GSIF for corner B in an infinite plate ($l_x/d_x$=0) is extrapolated. Here, the exact solution for one diamond-shaped inclusion in an infinite plate is used as a reference. Table 1 shows the results of two diamond-shaped inclusions in a plate which is showed in Fig.2 under tension $\sigma^\infty_y = \sigma$. From Table 1, it is seen that the FEM results for $E_I/E_M$=$10^{-2}$ coincide with the exact solutions of within the error of 1.0%. However, Table 2 shows that when $E_I/E_M = 10^2$, the FEM results have the largest error of about 9% compared with the exact solution.

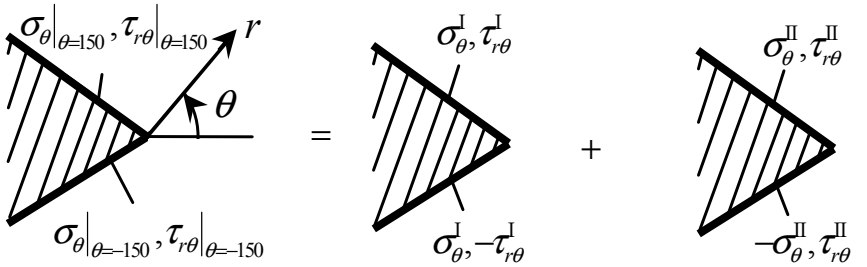


$$\sigma_\theta|_{\theta=150^\circ} = \sigma_\theta^{\mathrm{I}} + \sigma_\theta^{\mathrm{II}} \qquad \tau_{r\theta}|_{\theta=150^\circ} = \tau_{r\theta}^{\mathrm{I}} + \tau_{r\theta}^{\mathrm{II}}$$

$$\sigma_\theta|_{\theta=-150^\circ} = \sigma_\theta^{\mathrm{I}} - \sigma_\theta^{\mathrm{II}} \qquad \tau_{r\theta}|_{\theta=-150^\circ} = -\tau_{r\theta}^{\mathrm{I}} + \tau_{r\theta}^{\mathrm{II}}$$

Figure 3: Definition of interface stress $\sigma_\theta^{\mathrm{I}}$, $\tau_{r\theta}^{\mathrm{I}}$, $\sigma_\theta^{\mathrm{I}}$, $\tau_{r\theta}^{\mathrm{II}}$

Table 1(a): Results of $F_{\mathrm{I},\lambda_1,real}$ in Fig.2 ($E_I/E_M = 10^{-2}$)

| $l_x/d_x$ | | $F_{1,\lambda_1,FEM}$ | $F^*_{1,\lambda_1,BFM}$ | $\frac{F_{1,\lambda_1,FEM}}{F^*_{1,\lambda_1,BFM}}$ |
|---|---|---|---|---|
| 0 | $B, B'$ | 1.054 | 1.054 | 1.000 |
| 1/3 | $B$ | 1.069 | 1.068 | 1.001 |
| | $B'$ | 1.065 | 1.065 | 1.000 |
| 1/2 | $B$ | 1.095 | 1.090 | 1.005 |
| | $B'$ | 1.078 | 1.076 | 1.002 |
| 2/3 | $B$ | 1.155 | 1.148 | 1.011 |
| | $B'$ | 1.097 | 1.095 | 1.002 |

Table 1(b): Results of $F_{\mathrm{I},\lambda_1,real}$ in Fig.2 ($E_I/E_M = 10^2$)

| $l_x/d_x$ | | $F_{1,\lambda_1,FEM}$ | $F^*_{1,\lambda_1,BFM}$ | $\frac{F_{1,\lambda_1,FEM}}{F^*_{1,\lambda_1,BFM}}$ |
|---|---|---|---|---|
| 0 | $B, B'$ | 0.174 | 0.174 | 1.000 |
| 1/3 | $B$ | 0.172 | 0.175 | 0.982 |
| | $B'$ | 0.173 | 0.172 | 1.003 |
| 1/2 | $B$ | 0.169 | 0.185 | 0.915 |
| | $B'$ | 0.172 | 0.176 | 0.975 |
| 2/3 | $B$ | 0.224 | 0.206 | 1.087 |
| | $B'$ | 0.171 | 0.181 | 0.946 |

### *3.2 Results for a wedge-shaped defect restored by the composite resin when $E_I/E_M < 1$*

An example of maxillary second premolar with wedge-shaped defect restored by composite resin is considered. Then, a two-dimensional model as shown in Fig.4 is constructed for the finite element analysis. Human tooth model consists of enamel, dentin and composite resin as shown in Fig.4, and those elastic constants are assumed as shown in Table 8, however ,the elastic modulus of pulp is neglected.

When $E_I/E_M$<1, the stresses at $\theta$=0° are expressed in the following equations.

$$\tau_{r\theta}|_{\theta=0^\circ} = \frac{F_{r\theta}|_{\theta=0^\circ}}{r^{1-\lambda_2}} \; \sigma_\theta|_{\theta=0^\circ} = \frac{F_{\theta\theta}|_{\theta=0^\circ}}{r^{1-\lambda_1}}, \tag{21}$$

Figure 5 shows relation between $F_{\theta\theta}$ and magnitude of Pi (i=1∼14). When $E_I/E_M$ =300/1200. In Fig. 5, it is known that the tensile and compressive strength of enamel are in the ratio of 1 to 10 (see Table 3). Therefore tensile stress may be more harmful than compressive stress for enamel. The compressive strength about dentin is known as 213-380MPa. Although there is little study about the tensile strength of dentin, it has been told that it is about 1/7 of the compressive strength. Therefore tensile stress also may be more harmful than compressive stress for dentin. From Fig.5, it is found that the load $P_9$ may be most harmless because of the subtraction of the compressive due to the load $P_9$ and the tensile stress due to the bending moment. On the other hands, the loads $P_1$, $P_3$, $P_8$, $P_{10}$ acting perpendicular to the tooth axis are most harmful perhaps because the stress due to the bending moments become larger in those loads. If the occlusion can be adjusted as in the direction of $P_{11}$, the risk of fracture from the wedge-shaped defect may be reduced. On the other hands, the loads $P_1$, $P_3$, $P_8$, $P_{10}$ acting the vertical directions to the tooth axis are most harmful perhaps because the stress due to the bending moments become larger in those loads. On the other hands, the loads $P_1$, $P_3$, $P_8$, $P_{10}$ acting perpendicular to the tooth axis are most harmful perhaps because the stress due to the bending moments become larger in those loads. Fig.6 shows relation between $F_{\theta\theta}$ and magnitude of Pi (i=1∼14). When $E_I/E_M$=1000/1200. Similar conclusions can be seen from Fig.6.

### *3.3 Results for a wedge-shaped defect restored by the composite resin when $E_I/E_M > 1$*

Table 2 shows singular index of in Eq.1 of composite resin. When $E_I/E_M$ = 2000/1200, 2500/1200, $\lambda_2 = 1.0$, and therefore, the singular stress field is expressed by $K_{\mathrm{I},\lambda_1}$ only. Namely,

$$\tau_{r\theta}|_{\theta=150^\circ} = -\tau_{r\theta}|_{\theta=-150^\circ} = \frac{F_{r\theta}|_{\theta=150^\circ}}{r^{1-\lambda_1}}, \quad \sigma_\theta|_{\theta=150^\circ} = \sigma_\theta|_{\theta=-150^\circ} = \frac{F_{\theta\theta}|_{\theta=150^\circ}}{r^{1-\lambda_1}}, \tag{22}$$

Assume the intensity $F_{\theta\theta}$ is the most harmful for the fracture at the corner of wedge-shaped inclusion. From Fig.7, it is found that the load $P_{11}$ may be the most harmless. On the other hand, the loads $P_1$, $P_3$, $P_8$, $P_{10}$ are harmful because they cause tensile stresses at the interface. If the occlusion can be adjusted as in the direction of $P_{11}$, the risk of extension or fracture from the restored wedge-shaped defect may be reduced.

## 4 Conclusions

General stress intensity factors for two diamond-shaped inclusions in a plate are investigated for validating the current solution method. Furthermore, singular stress field for corner B of wedge-shaped defect restored by the composite resin was researched by using the Finite Element Method in this paper. The conclusions can be made in the following way:

1. For two diamond-shaped inclusions in a plate (shown in Figure 2), the GSIF results for $E_I/E_M$=$10^{-2}$ corroborate the exact solutions of Body Force Method with the error no more than 1.0%. Moreover, when $E_I/E_M$=$10^2$, the FEM results have the largest error of about 9%.

2. The intensity of the singular stress was investigated with varying the position and direction of the occlusal force. As shown in Table. 4, it is found that $P_3$ is the most dangerous load for any composite resin and dentin ratio $E_I/E_M$. However, loads $P_9$, $P_{11}$ and $P_{14}$ are the safest load for the corner B under different $E_I/E_M$ ratio respectively.

## References

**Bream, M. et al.** (1992): Stress inducedcervical lesions, *J Prosthet Dent*, Vol.67, pp.718-722.

**Chen, K.K. et al.** (2000): Effects of Occulusion on the Formation of Wedge-shaped Defect-Cervical region Strain along Tooth Axis, *The Japanese Journal of Conservative Dentistry* (in Japanese) , Vol.43, pp.870-876.

**Chen, D., Nishitani, H.** (1991): Transaction of JSME Vol. 57-534, p.366-372.

**Graehn, G., Muller, H.H.** Wedge-shaped defects of Teeth of Animals, *Dtsch Zahn Mund Kiefrheilkd*, Vol.79, pp.441-449.

**Lee, W.C., Eakle, W.S.** (1984): Possible role of tensile stress in the etiology of cervical lesions of teeth, *J Prosthet Dent*, Vol.52, pp.374-380.

**Miller, W.D.** (1907): Experiments and observations on the wasting of tooth tissue variously designated as erosion, abrasion, chemical abrasion, denudation, etc, Den Cosmos, Vol.49, pp.1-23, pp.109-124, pp.147-225.

**Noda, N., Kawashima, Y., Oda, K.** (1996): Transaction of JSME Vol.62-598, p.1456.

**Tanaka, H. et al.** (1993): Studies on the Cervical Loss of Tooth Structure - Japanese Teeth before and during the Edo Era, The First Report: Edo Era(1), *The Japanese Journal of Conservative Dentistry*, Vol.36, No.1, pp.287-294.